Drug Design, Development and Therapy

Dovepress
Taylor & Francis Group

Open Access Full Text Article

ORIGINAL RESEARCH

Sustained Release of Ropivacaine from Adhesive Injectable Microbubbles with Contrast-Enhanced Ultrasonography in Pain Management: An Animal Model Study

Hui-Jie Shang[1,2,*], Hao-Tian Ye[1,*], Cai-Bao Yue[1,3], Mu-Huo Ji[4], Han-Wen Gu[1], Wei-Tong Pan[1,3], Pan-Miao Liu[1], Jian-Jun Yang[1]

[1]Department of Anesthesiology, Pain and Perioperative Medicine, the First Affiliated Hospital of Zhengzhou University, Zhengzhou, 450052, People's Republic of China; [2]Department of Anesthesiology, New Jersey Medical School, Rutgers, the State University of New Jersey, Newark, New Jersey, USA; [3]Neuroscience Research Institute, Zhengzhou University Academy of Medical Sciences, Zhengzhou, 450052, People's Republic of China; [4]Department of Anesthesiology, the Second Affiliated Hospital, Nanjing Medical University, Nanjing, 210003, People's Republic of China

*These authors contributed equally to this work

Correspondence: Pan-Miao Liu; Jian-Jun Yang, Department of Anesthesiology, Pain and Perioperative Medicine, the First Affiliated Hospital of Zhengzhou University, No. 1 Jianshe East Road, Zhengzhou, Henan Province, People's Republic of China, Email liupan3374@126.com; yjyangjj@126.com

Background: Perioperative pain poses a significant challenge for surgical patients, with regional anesthesia commonly employed for postoperative pain relief. However, the utility of regional anesthesia is limited by the lack of real-time visualization during drug delivery and the rapid diffusion of anesthetics, which result in imprecise targeting and short duration of analgesia.

Methods: An innovative ultrasound-guided drug sustained-release capsules were fabricated by bioinspired adhesive polylactic-co-glycolic acid (PLGA) loaded with ropivacaine microbubbles (APRMs). Ropivacaine release and ultrasonographic experiments of APRMs were conducted in vitro. For in vivo evaluation, a total of 127 adult male Sprague–Dawley rats (200–250 g) were used. Then, incision surgery and SNI-induced neuropathic pain were conducted for adult male rats to verify the ropivacaine release of APRMs in vivo. Ultrasound imaging was performed to confirm the ultrasonic visualization of APRMs. The in vivo fluorescence imaging experiment was conducted for the adhesion property of APRMs. Finally, systemic toxicity and tissue reaction were histologically evaluated.

Results: APRMs achieved real-time visualization during drug delivery and significantly prolonged antinociceptive effects, maintaining mechanical analgesia for 9 days and thermal analgesia for up to 15 days, whereas free ropivacaine produced only transient effects (mechanical: approximately 24 h; thermal: approximately 4 h). Histological assessments revealed no toxicity or adverse tissue reactions, underscoring the safety of APRMs.

Conclusion: APRMs represent a novel and promising strategy for pain management by integrating sustained anesthetic release, bioinspired adhesive properties for prolonged retention, and contrast-enhanced ultrasonography (CEUS) for real-time visualization. While these findings are encouraging, further in vivo validation and extended preclinical studies will be essential to confirm safety and efficacy before considering translation into clinical practice.

Keywords: pain management, microbubbles, ropivacaine, polydopamine

Introduction

Effective perioperative pain management remains a major clinical challenge. Systemic analgesics such as opioids, commonly administered orally or intravenously, can provide effective pain relief but are accompanied by substantial safety concerns, including abuse potential, addictive properties, and intoxication-associated morbidity and mortality.[1,2] By contrast, ultrasound-guided nerve blocks, a regional anesthesia technique, offer an alternative by selectively blocking

https://doi.org/10.2147/DDDT.S532749
Received: 7 April 2025
Accepted: 9 February 2026
Published: 27 February 2026

nerve excitation and conduction, potentially reducing these risks.[3–5] However, despite their advantages, nerve blocks are limited by a relatively short duration of action, technical complexity, and risks such as nerve injury, local anesthetic systemic toxicity, and incomplete blockade.[6,7] These shortcomings underscore the need for innovative strategies that can prolong analgesic duration, reduce complications, and allow real-time monitoring of drug delivery.

Most existing research has centered on enhancing imaging technology,[8] with less emphasis on developing contrast agents for local anesthetics. The utilization of microbubble contrast agents, though effective for enhancing procedural visualization in echocardiography and neural catheter placement,[9] is constrained by potential complications associated with inadvertent air injection into vascular or intrathecal spaces, which may adversely affect regional anesthesia performance. Furthermore, most local anesthetics provide only short-term relief after a single injection, insufficient for extended pain management.[10] Current strategies to prolong nerve block duration, such as higher single doses, multiple injections with adjuvants, or implanted delivery systems for continuous infusions,[11–13] are often hindered by rapid drug diffusion, resulting in low therapeutic efficacy. This underscores the need for an ultrasound-guided, sustained-release formulation that enhances visibility, duration, and safety in regional anesthesia.[14]

To address these issues, an advanced polymeric microcarrier system with integrated contrast properties was developed for regional anesthesia. Polymer microspheres and nanoparticles have become essential components of drug delivery platforms, offering enhanced drug loading and controlled release properties.[15] PLGA, having received the FDA and EMA approval for various clinical uses, is particularly notable for its biocompatibility, biodegradability, and sustained drug delivery capabilities.[16,17] The integration of local anesthetics into PLGA-based microspheres has been shown to maintain sustained drug release, resulting in prolonged pain relief during regional anesthesia procedures.[18–20] Nevertheless, existing research has predominantly emphasized the characterization of pharmaceutical release kinetics,[21–23] overlooking additional features such as visualization and targeted tissue adhesion.

In this study, we engineered mussel protein inspired adhesive PLGA-ropivacaine microbubbles (APRMs) with a surface coating material for PLGA microbubbles containing encapsulated ropivacaine to achieve sustained release, contrast-enhanced ultrasonography, and strong tissue adhesion (Figure 1). Ropivacaine, a potent local anesthetic, has gained widespread acceptance in pain management due to its efficacy and safety profile.[24] Polydopamine, inspired by mussels, is a biocompatible coating material known for its strong adhesion to various surfaces;[25,26] Polydopamine was selected as the adhesive component because it is a bioinspired material that exhibits strong and universal adhesion under physiological conditions, superior biocompatibility, and the ability to form stable surface coatings. Compared with other adhesion materials, such as polylysine or synthetic catechol derivatives, polydopamine provides more reliable adhesion and better tissue compatibility, making it particularly suitable for enhancing the retention of drug delivery systems at the target site while minimizing potential immune responses. Consequently, APRMs are expected to exhibit robust tissue-adhesion capabilities. Additionally, PLGA's capacity to encapsulate ropivacaine enables APRMs to achieve sustained drug release, extending the duration of analgesia. Significantly, the APRMs demonstrated contrast-enhanced ultrasonography (CEUS) capabilities, attributable to their unique hollow microstructural configuration. Furthermore, the APRMs demonstrate a reduced potential for systemic toxicity through minimized peak plasma drug concentrations. Therefore, the present study aimed to develop adhesive injectable microbubbles (APRMs) as a novel platform for sustained release of ropivacaine, integrating bioinspired adhesive properties for prolonged tissue retention with CEUS for real-time visualization. We further evaluated their analgesic efficacy, biocompatibility, and imaging properties in both in vitro and in vivo models. Overall, APRMs offer precise, safe, and sustained analgesic effects, highlighting their potential as an extended-release local anesthetic in pain management.

Materials and Methods

Material

Polylactic-co-glycolic acid (PLGA) (38,000–54,000 MW) was sourced from Adamas-beta (Shanghai, China). Dichloromethane (DCM) was provided by Sinopharm (Shanghai, China). Polyvinyl alcohol (PVA) (87–89% hydrolysis, ~31,000 MW) and Cy5.5 NHS ester were obtained from Aladdin (Shanghai, China). Ropivacaine base was obtained from Macklin (Shanghai, China), and its hydrochloride formulation (1% w/v) from AstraZeneca AB (Sweden).

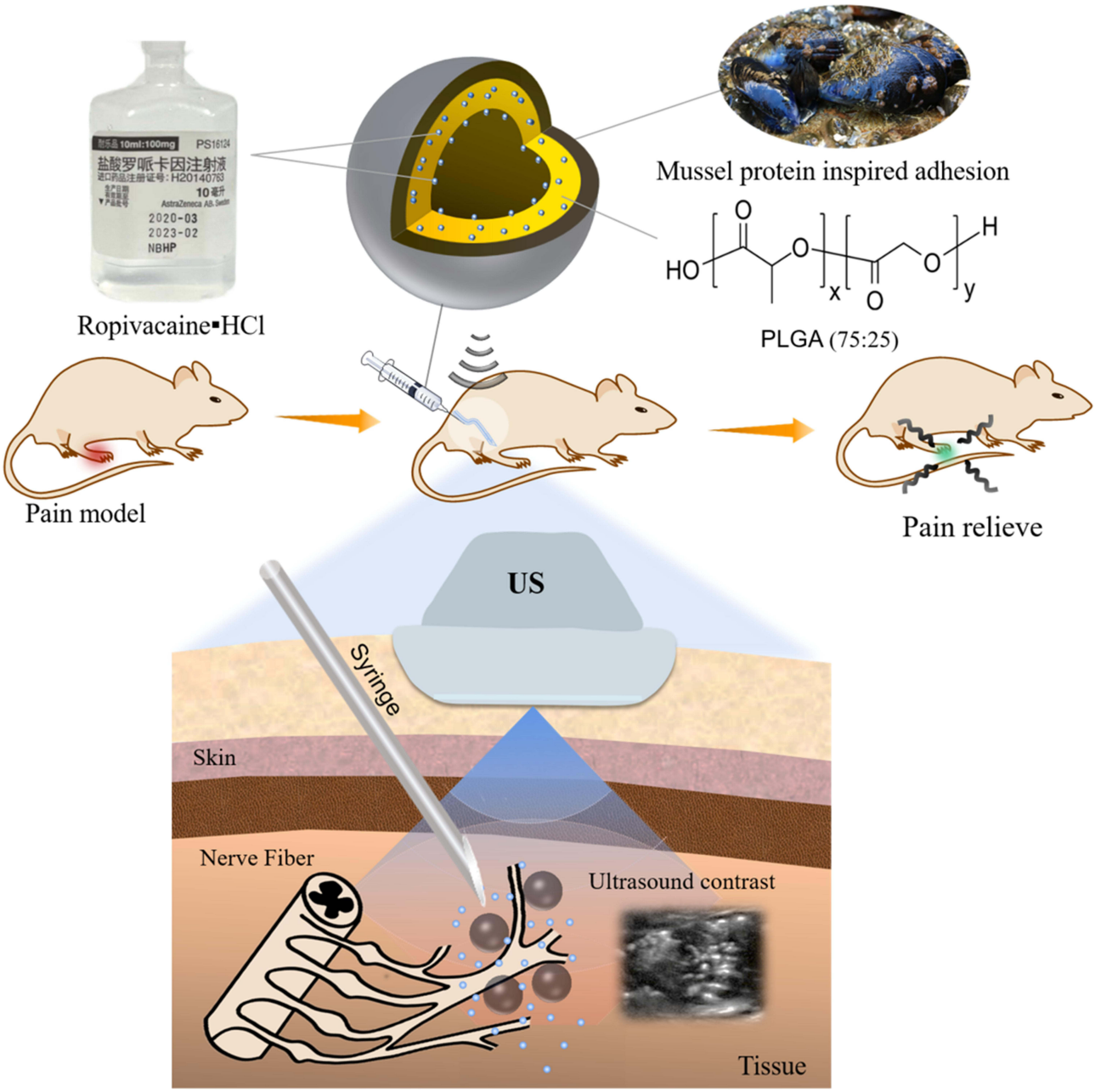

Figure 1 Schematic illustration of mussel protein inspired adhesive injectable microbubbles applied in surgical incision pain and neuropathic pain induced by SNI.

Preparation of APRMs

APRMs were produced via a water-in-oil-in-water (w/o/w) emulsion-based solvent evaporation method. First, 300 mg PLGA and 200 mg ropivacaine base were dissolved by 6 mL methylene chloride. After well-mixed, 4 mg ropivacaine hydrochloride was added under stirring at 200 rpm for 1 hour. Subsequently, 45 mL 1.5% PVA solution was introduced, then the mixture was stirred at 60 rpm for 12 hours to obtain PRMs. Then they were washed by centrifugation at 2000 rpm for 10 minutes with deionized water for 3 times, freeze-dried with a lyophilizer (Alpha 1–2 LD plus, Martin Christ, Germany). To prepare APRMs, 0.1 g of PRMs was dispersed in a solution containing 20 mg dopamine and Tris buffer (10mM, pH = 8.5), followed by continuous stirring (100 rpm) for 18 hours. The APRMs were purified by 3 centrifugation cycles. Cy5.5-loaded PRMs or APRMs were prepared by dissolving Cy5.5 NHS ester in the methylene chloride solvent initially.

https://doi.org/10.2147/DDDT.S532749

Ropivacaine Loading on APRMs

0.1 g APRMs were dispersed in 10 mL anhydrous ethanol to assess EE and DLE. After vortex mixing, the sample was processed with centrifugal force at 8000 rpm to separate any insoluble residues for 5 minutes. The concentration of ropivacaine was measured and quantified. EE and DLE were determined:

EE (%) = (mass of ropivacaine encapsulated in PLGA microbubbles / total mass of ropivacaine) × 100%.

DLE (%) = (mass of encapsulated drug / total mass of components in the system) × 100%.

Release of Ropivacaine from APRMs in vitro

A total of 100 mg APRMs were enclosed in a dialysis tube (MD25-3500, Viskase, USA), which was then immersed in 5 mL saline. The experimental system was incubated at physiological temperature (37°C) using a thermostatic orbital shaker (New Brunswick™ Innova® 40, Eppendorf, USA). At predetermined intervals, the dialysis tube was transferred to new solution. Ropivacaine quantification was performed by high performance liquid chromatography (LC-20AT system, Shimadzu Corporation, Japan).

Animal Preparation

Adult male Sprague-Dawley rats were procured from Sibeifu Biotechnology Company (Beijing, China). A total of 127 adult male Sprague-Dawley rats (weight: 220 ± 15 g, mean ± SD) were used in this study (Figure S1). They were maintained individually with unlimited water and food. The ambient temperature was regulated at 23 ± 2°C, and the lighting followed a natural light-dark cycle. The study followed NIH guidelines and was approved by Zhengzhou University's Institutional Animal Care and Use Committee (ZZU-LAC2021011904). Every effort was taken to reduce the number of animals utilized and to minimize any potential distress.

Perisciatic Nerve Injection

The perisciatic nerve was accessed using a 20-gauge needle attached to a 1-mL syringe under isoflurane-induced anesthesia and the surgical field around the right hind limb was shaved and disinfected with povidone–iodine solution. Following identification of the greater trochanter, the needle was positioned posteromedially until bone contact was established, after which 1 mL of the test solution was slowly injected. All procedures were performed under aseptic conditions to minimize the risk of infection.

Incisional Pain Model

The incision pain model was established using Brennan's plantar incision technique.[27] Male rats were anesthetized with 2–3% isoflurane through a nasal delivery apparatus. The plantar surface was sterilized for three times. A 1-cm incision was made 0.5 cm from the heel, cutting through the skin, fascia, and muscle. The plantaris muscle was gently lifted, incised lengthwise, and repositioned. Bleeding was controlled using sterile gauze, and the wound was closed with 2–0 nylon sutures. Rats recovered from anesthesia before being returned to their cages. Daily inspections were conducted, and rats with infections or wound complications were excluded.

SNI-Induced Neuropathic Pain Model

The SNI procedure was conducted following established methods.[28] Rats were anesthetized using 2–3% isoflurane, and a lateral thigh incision exposed the sciatic nerve and its branches. Both the common peroneal nerve and tibial nerve branches were surgically ligated with 5.0 silk, cut distally, and 2–4 mm of nerve ends were removed, while the sural nerve remained intact.

Behavioural Tests

Rats underwent an acclimatization period of at least three days in the testing environment. Paw withdrawal threshold (PWT) was measured with von Frey filaments, and the 50% PWT was determined with the up-down method.[29] Prior to testing, the rats were positioned in chambers for 30 minutes. The experiment commenced by applying a 2.0 g filament

perpendicularly to the plantar area of the hind paw, continuing until the filament formed an S-shaped curve for 3–5 seconds. A paw withdrawal or licking response was recorded as positive, prompting the use of a smaller filament. A lack of response was noted as negative, and a larger filament was applied. Testing ceased under the following conditions: 1) no response at the maximum filament strength (15 g); 2) a positive response at the minimum filament strength (0.4 g); 3) four consecutive tests after a response change; or 4) a total of nine measurements. Intervals between tests exceeded 5 minutes.

Paw withdrawal latency (PWL) was measured with a plantar analgesia tester (7370, Ugo Basile, Comerio, Italy), following standardized protocols.[30] A radiant heat stimulator was positioned beneath a transparent glass platform to deliver thermal stimuli to the plantar surface of the hind paw. Three trials were carried out, with intervals of over 5 minutes. The mean was determined from three consecutive measurements. All behavioral tests were conducted in a randomized and blinded manner. Randomisation: All animals were randomly assigned to experimental groups using a computer-generated random number sequence (using www.randomizer.org) created by an investigator not involved in behavioral testing, data acquisition, or analysis. Randomisation was applied before any surgical procedure (plantar incision or SNI), before drug preparation, and before perisciatic injection to prevent selection bias. Allocation concealment: The investigator who performed the randomization was responsible for implementing allocation concealment. The treatments (Vehicle, PLGA, RVC, PRMs, APRMs) were prepared by a separate individual and dispensed into identical, unmarked syringes. Each syringe was labelled only with the corresponding animal's study identifier. The surgeon performing the perisciatic nerve injection received the syringe labelled with the animal's ID and was thus unaware of the group assignment. Allocation was concealed from the surgeons and investigators from the moment of group assignment until after all data collection and analysis were complete. This prevented any conscious or subconscious bias during treatment administration and outcome assessment. Blinding procedures: Blinding was maintained for all key personnel involved in the experimental procedures and data handling. As described under allocation concealment, this individual received pre-loaded, identically appearing syringes labelled only with animal IDs. They had no knowledge of the group allocation key. They were provided with the animals in a random order and were only aware of the animal's unique ID. They had no access to the group allocation list during testing. The testing environment and apparatus were standardized to ensure consistency.

Locomotor Dysfunction Test

Locomotor function was assessed using established methods.[31] 1) Placing reflex: Rats were placed with their hind limbs lower than their forelimbs, allowing the dorsal side of the hind paws to touch a table The ability to reflexively place the hind paws on the table surface was recorded. 2) Grasping reflex: Rats were positioned on a wire grid, and their ability to grasp the wires with their hind paws upon contact was documented. 3) Righting reflex: Rats were placed on their backs on a flat surface, and their ability to immediately return to an upright position was observed. Each reflex was evaluated over five trials, with scores based on the number of normal responses recorded.

HE Staining

At the predetermined time point, rats were euthanized via decapitation. Sciatic nerve samples and major organs were collected. Paraffin sections prepared for HE staining were dewaxed, rehydrated, and sequentially stained with haematoxylin and eosin. After dehydration and sealing, the sections were examined under a microscope.

Plasma Samples Testing

Plasma concentrations of ropivacaine were analyzed with high-performance liquid chromatography (HPLC). Blood samples were collected from the caudal veins at different time course following sciatic nerve injection of ropivacaine or APRMs. Plasma was separated by centrifugation. To extract the sample, 400 μL acetonitrile was mixed with 200 μL plasma with sonication and centrifugation. The supernatant was analyzed with an HPLC system equipped with a C18 column (5 μm, 4.6×250 mm), with detection at a wavelength of 263 nm.

The HPLC method was fully validated according to standard bioanalytical guidelines. Specificity was confirmed by analyzing blank plasma and plasma spiked with ropivacaine, ensuring no interference from endogenous components.

Linearity was established over a concentration range of 10–5000 ng/mL, with a correlation coefficient (R^2) ≥ 0.999. Accuracy and recovery were evaluated at low, medium, and high concentrations, yielding recovery rates of 95–105%. Precision, assessed both intra-day and inter-day, showed relative standard deviations (RSD) <5%. The lower limit of quantification (LLOQ) was 10 ng/mL, with a signal-to-noise ratio >10, and accuracy and precision within ±20%. Below the lower limit of quantification (BLOQ) concentrations occurring prior to Cmax were imputed as LLOQ/2, whereas BLOQ values occurring after Cmax were treated as missing. Stability of ropivacaine in plasma was verified under short-term room temperature, long-term storage at −80°C, and multiple freeze–thaw cycles.

Characterization

Ropivacaine concentrations were quantified via HPLC. Solution-state morphological characteristics of PRMs and APRMs were documented using a commercial smartphone imaging system (Huawei Mate40 Pro). Ultrasonic imaging was performed using a portable ultrasound device (Sonosite Edge II, FUJIFILM Sonosite, Inc., USA). In vivo imaging was conducted with an IVIS Spectrum system (PerkinElmer, Massachusetts, USA). Neural microstructure characterization, including myelinated fiber quantification and axonal ultrastructure assessment, was conducted with a Transmission Electron Microscope (TEM, Hitachi HT7700, Japan).

Endpoint Hierarchy

We pre-specified one primary endpoint for each experimental question based on biological relevance and sensitivity of the measurement, prior to data analysis. For in-vitro release experiments, the cumulative release (%) was designated as the primary endpoint. For in-vivo pharmacokinetic evaluation, the plasma concentration was designated as the primary endpoint, as it most accurately reflects systemic exposure in a sustained-release formulation. For tissue adhesion studies, the primary endpoint was fluorescence intensity within a predefined region of interest (ROI) over time, representing adhesion retention at the injection site. ROIs were manually delineated over the perisciatic nerve region corresponding to the injection and adhesion site, guided by the area of maximal Cy5.5 signal intensity. To ensure longitudinal consistency, identical ROI size and placement were applied across all time points within the same animal. For evaluation of analgesic efficacy following perisciatic nerve injection, paw withdrawal threshold (PWT) and paw withdrawal latency (PWL) were designated as the primary endpoints, as they are the most sensitive and widely adopted indicators of postoperative mechanical and thermal hypersensitivity. One primary endpoint per experimental question (as listed above) and the other variables are secondary.

Unit of Analysis

The experimental unit was defined a priori for each endpoint as the smallest biological entity to which an independent treatment was applied and from which biological inference was drawn. Technical replicates were not treated as independent biological observations. For in vivo experiments, including behavioral pain assessments (PWT and PWL), locomotor reflex testing, in vivo imaging, pharmacokinetic measurements, and histological analyses, the individual animal was considered the experimental unit. Repeated measurements obtained from the same animal over time were treated as within-subject observations and were analysed using mixed-effects models. For behavioural testing, multiple trials obtained within the same session (eg, three PWL measurements or repeated von Frey stimulations) were averaged to generate a single value per animal per time point prior to statistical analysis. For locomotor reflex testing, five repeated trials per animal were summarised as composite scores and analysed at the animal level. For imaging analyses, quantitative metrics were extracted from predefined regions of interest (ROIs). When multiple ROIs or image frames were obtained from the same animal at a given time point, values were averaged or modelled as repeated measures nested within the animal, as appropriate. For pharmacokinetic analysis, serial plasma samples collected from the same animal were treated as repeated measures. Pharmacokinetic parameters were estimated at the individual-animal level and used for between-group comparisons. For histological and ultrastructural analyses, multiple sections or microscopic fields obtained from the same animal were considered technical replicates and were summarised to yield a single animal-level value prior to statistical analysis. For in vitro experiments, including drug loading, release, and material characterisation, the experimental unit was an independently prepared microsphere batch. Repeated assay measurements from the same

preparation were treated as technical replicates and were averaged prior to analysis or incorporated as within-unit repeated measures where appropriate.

Statistical Analysis Plan

Statistical analysis was performed using SPSS, version 26.0 (IBM SPSS), R statistical software, version 4.2.0 (R Project for Statistical Computing) and GraphPad Prism 8.0 (GraphPad Software, USA). Animals were randomly assigned via computer-generated lists; all behavioral scoring and analyses were performed by investigators blinded to group allocation.

The Shapiro–Wilk test was used to evaluate the normality of the data. The homogeneity of variances was assessed with the F-test (for pairwise comparisons) and the Brown-Forsythe test (for multiple groups). The outcomes of locomotor function scores (placing, grasping and righting) at different time points were analyzed with a linear mixed-effect model (LMM) using repeated measures. Treatment group, time, group×time interaction were included as fixed covariates. Random intercept and slope were modeled for each rat. Results for the analyses are reported as mean with S.E.M. for score, and mean difference with 95% CIs for pairwise comparisons between groups. The treatment-by-time interaction was first tested at a two-sided significance level of 0.05. If the interaction was statistically significant, treatment effects were estimated separately at each time point. Post-hoc pairwise group comparisons derived from the LMM were adjusted using Tukey's method. For other outcomes analyzed using LMMs (eg, in vivo imaging measures), post-hoc pairwise comparisons were likewise adjusted using Tukey's method. To account for multiplicity across distinct behavioral pain-related endpoints (PWT and PWL), we applied the Benjamini–Hochberg false discovery rate (FDR) correction at 5% to the set of p-values corresponding to the primary treatment effects for these endpoints. The FDR procedure was applied only across these separate behavioral endpoints and not to any post-hoc pairwise comparisons within LMM analyses. Significance was established at $p < 0.05$ for all analyses.

Results

Preparation of APRMs

The APRMs were effectively synthesized through a water-in-oil-in-water (w/o/w) emulsion-based solvent evaporation approach (Figure 2a). Fourier Transform Infrared (FT-IR) analysis (Figure 2b) validated PRMs' chemical composition, showing ropivacaine-specific peaks: aromatic ring vibrations at 1628 cm^{-1} and 3001 cm^{-1}, and NH stretching at 1512 cm^{-1}. The Scanning Electron Microscopy (SEM) images confirmed the uniform spherical morphology of the synthesized PRMs (Figure 2c). After freeze-drying, PRMs underwent surface modification via dopamine hydrochloride polymerization in Tris-buffer solution, producing APRMs with a polydopamine coating layer (Figure 2d). Additionally, enhanced magnification SEM analysis showed the hollow, spherical morphology of the PRMs. Ropivacaine levels were quantified through absorbance measurement at 263 nm, using a standard calibration curve for reference (Figure S2). Quantitative analysis revealed that APRMs exhibited an encapsulation efficiency (EE) of 23.1 ± 1.1% and a drug loading efficiency (DLE) of 54.5 ± 3.6%. Contact angle measurements illustrated a notable increase in hydrophilicity upon polydopamine coating, with PRMs exhibiting an 80.202° contact angle, reduced to 18.512° on APRMs (Figure 2e). The obtained results provide confirmation of successful APRMs synthesis through polydopamine modification of PRMs. FT-IR spectroscopic analysis (Figure 2f) of ropivacaine, PRMs, and APRMs provided additional confirmation of successful polydopamine surface modification on PRMs because the characteristic peaks at 1284 cm^{-1} attributed to the stretching vibration of phenolic CO appeared from polydopamine in APRMs. Size measurements from SEM indicated that the diameter of APRMs was 29.64 ± 9.78 μm (Figure 2g). Collectively, these findings substantiate the successful synthesis of APRMs featuring hollow spherical morphology, efficient ropivacaine encapsulation, and a bioinspired polydopamine adhesive coating.

In Vitro Behaviors

The sustained release properties were initially evaluated through in vitro drug release studies. The release behavior of ropivacaine from PRMs (Figure 3a) was sustained for about 16 days (Figure 3b), reaching a maximum release of 90.88%

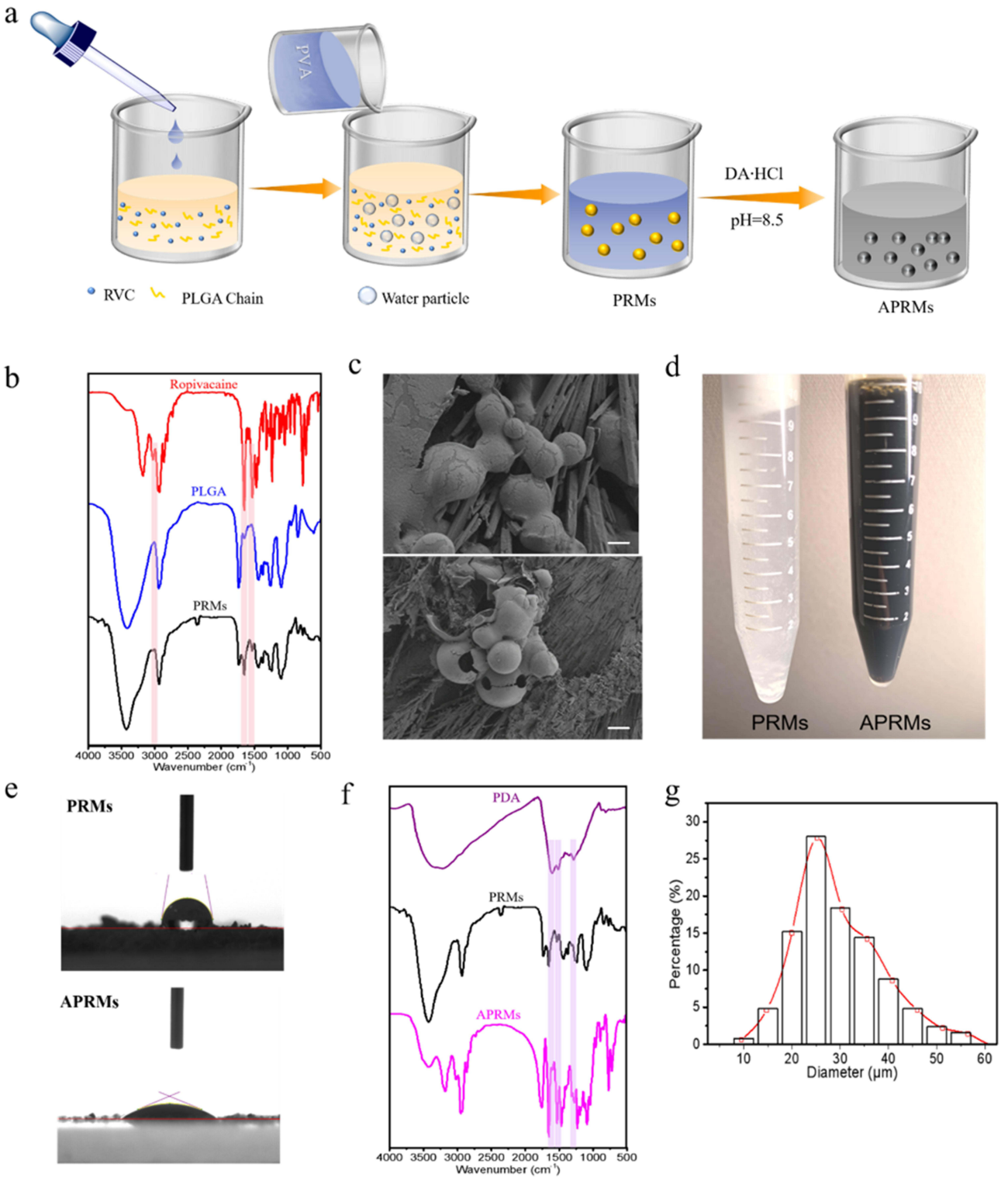

Figure 2 (**a**) Schematic illustration of the production process for APRMs. (**b**) FT-IR spectral characterization. (**c**) SEM characterization of PRMs. Insert bar is 2 μm for the top image and 20 μm for the bottom image. (**d**) Photograph of PRMs and APRMs in PBS solution. (**e**) Measurement of the contact angle of PRMs and APRMs. (**f**) FT-IR spectroscopy of polydopamine, PRMs and APRMs. (**g**) Size distribution histograms of APRMs; n=125.

of the total loaded drug (Figure 3c). In comparison, APRMs (Figure 3d) showed sustained ropivacaine release over approximately 20 days (Figure 3e), achieving a maximum release of 96.4% (Figure 3f). A significant disparity in initial release kinetics was observed, with PRMs demonstrating significantly higher ropivacaine release rates compared to APRMs during the first 48 hours (Figure 3c,f), presumably attributable to the diffusion-limiting properties of the

https://doi.org/10.2147/DDDT.S532749

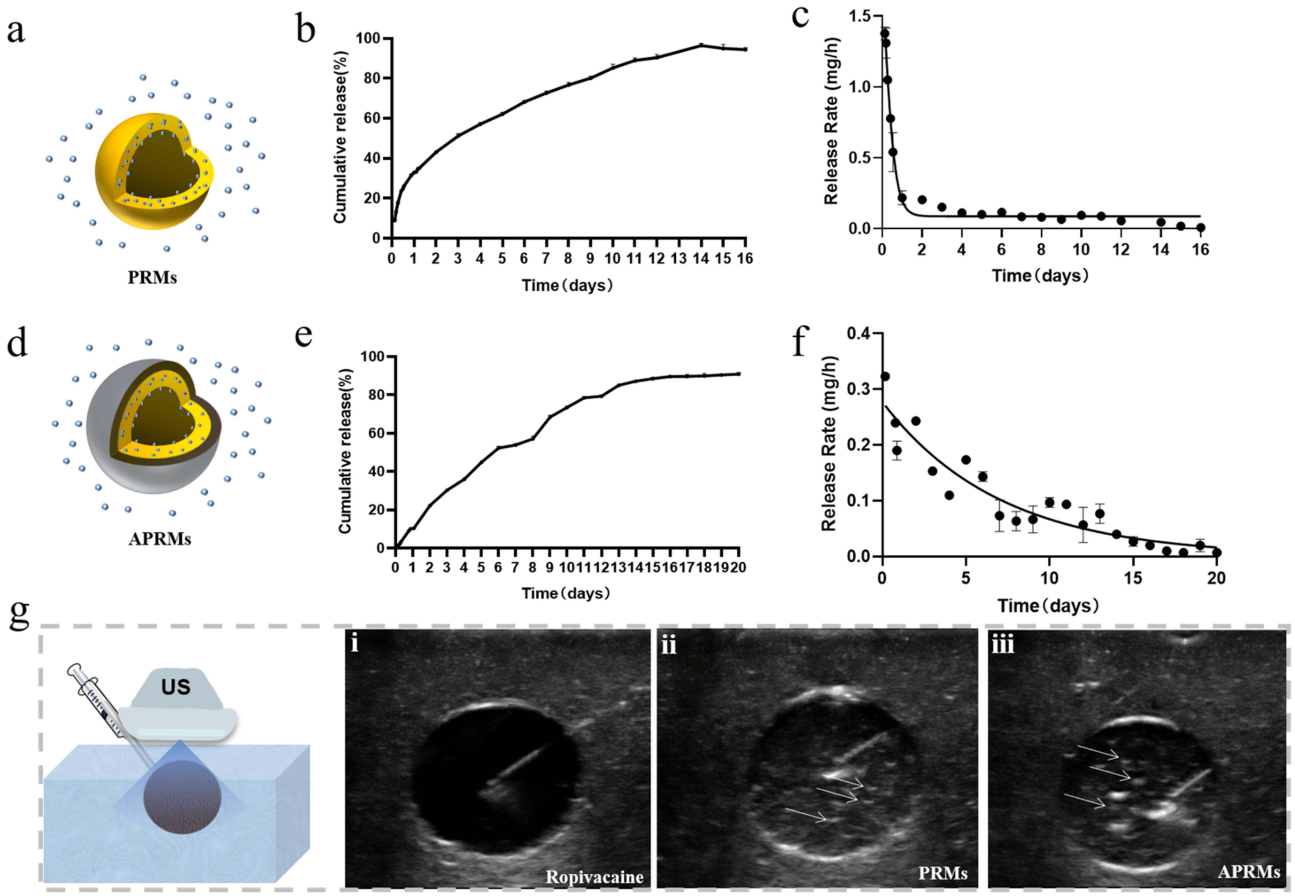

Figure 3 (**a**) Schematic diagram of ropivacaine release from PRMs in vitro. (**b**) Cumulative in vitro release behavior of ropivacaine from PRMs. (**c**) Release rate from PRMs in vitro. (**d**) Schematic diagram of ropivacaine release from APRMs in vitro. (**e**) Cumulative in vitro release behavior of ropivacaine from APRMs. (**f**) Release rate from APRMs in vitro. (**g**) B-mode ultrasound imaging analysis in agarose gel blocks. (i) ropivacaine, (ii) PRMs, (iii) APRMs. The white arrows indicate the microbubbles visualized under ultrasound. Data represent mean ± SEM from 6 independent biological experiments (**b, c, e, f**).

polydopamine coating on APRMs. Furthermore, APRMs, with their hollow spheroidal structure, exhibited contrast-enhanced ultrasound (CEUS) capabilities under ultrasound guidance. To validate this observation, they were individually administered into agarose gel matrices for ultrasonographic evaluation, including ropivacaine, PRMs, and APRMs (Figure 3g). Distinct imaging patterns were observed, with ropivacaine appearing as a hypoechoic zone and both APRMs and PRMs demonstrating hyperechoic characteristics with well-defined particulate morphology. Interestingly, APRMs (Video S1) maintained longer suspension stability at the administration site compared to PRMs (Video S2), likely due to the increased hydrophilicity and dispersibility provided by the polydopamine coating on APRMs. These results demonstrate that APRMs provide both sustained drug release and enhanced ultrasound contrast in vitro. The outstanding ultrasonographic properties of APRMs enable precise drug localization, thereby optimizing the accuracy and effectiveness of regional anesthesia procedures.

In vivo Behaviors

The release profile of APRMs in vivo is illustrated in Figure 4a. Firstly, plasma ropivacaine concentrations were monitored pre- and post- perisciatic nerve administration (Figure 4b). As shown in Figure 4b, the plasma concentration peaked at 20 minutes post-injection and dropped to undetectable levels within 24 hours in the free ropivacaine group. In contrast, APRMs demonstrated extended-release properties, maintaining plasma ropivacaine concentrations of approximately 200–600 ng/mL from 10 minutes to day 3 post-injection, with gradual decline to around 80 ng/mL by day 14, remaining detectable throughout this period, whereas free ropivacaine formulation rapidly declined to undetectable levels within day 1. Notably, the maximum plasma concentration of ropivacaine in the APRMs treatment group was

https://doi.org/10.2147/DDDT.S532749

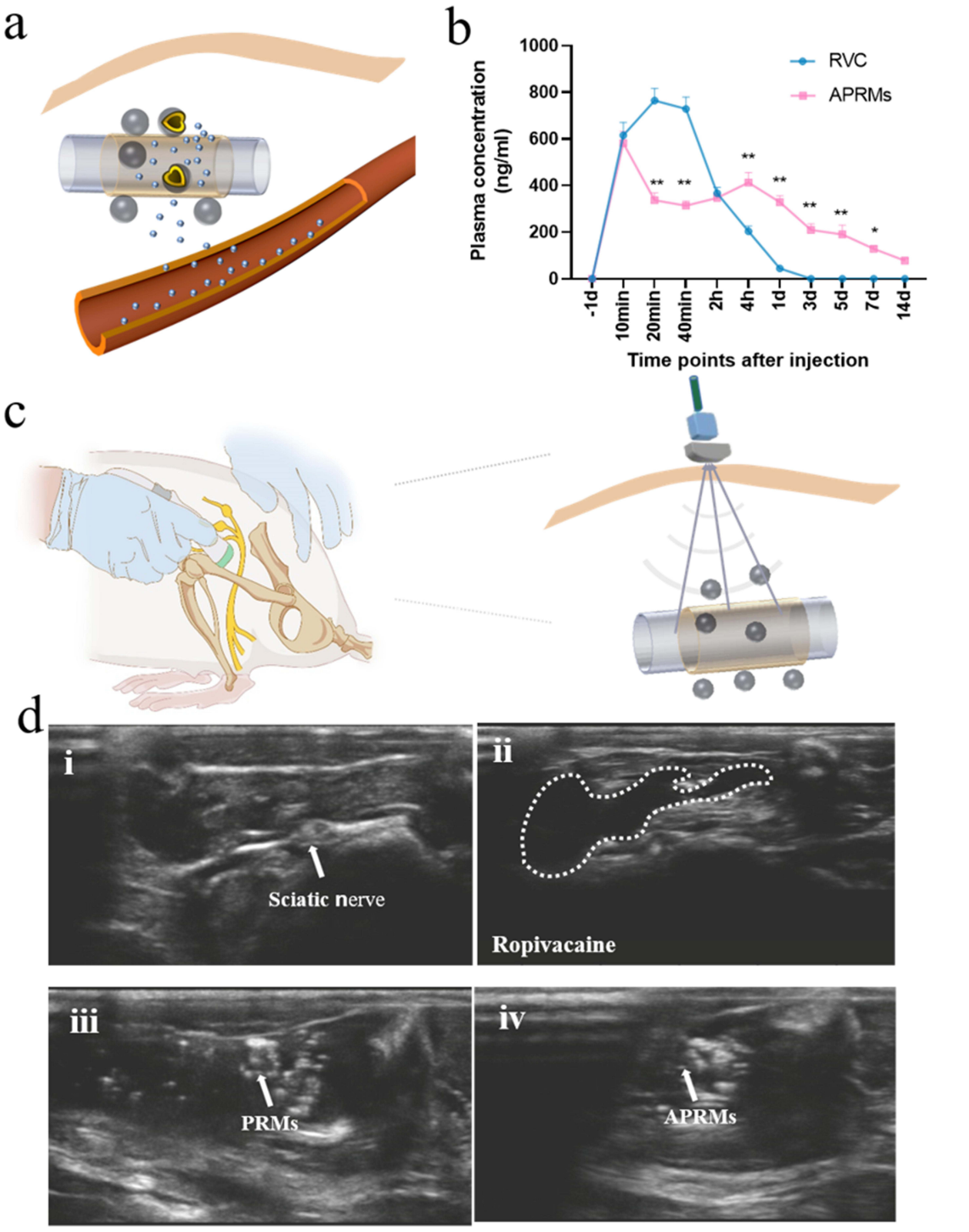

Figure 4 (**a**) Schematic diagram of ropivacaine release from APRMs in vivo. (**b**) Pharmacokinetic profiles of ropivacaine plasma concentrations. *P<0.05 or **P<0.01 comparison between the APRMs group and the free ropivacaine group. n=6 rats/group. (**c**) Graphical depiction of nerve block with ultrasound guidance. (**d**) (i) B-mode ultrasound image showing the target sciatic nerve in an SD rat. The white arrows indicate the target sciatic nerve. (ii–iv) B-mode ultrasound images of different samples in vivo: (ii) free ropivacaine. The dotted white marked area indicates the injected ropivacaine. (iii) PRMs. The white arrows indicate the microbubbles released from PRMs. (iv) APRMs. The white arrows indicate the microbubbles released from APRMs.

https://doi.org/10.2147/DDDT.S532749

significantly reduced compared to the free ropivacaine formulation, highlighting the excellent sustained-release performance of APRMs (Supplementary Table 1). This sustained-release capability also suggests that APRMs offer better adhesion and safety for surrounding visceral organs.

Next, the CEUS properties were evaluated in vivo. Using SD rat sciatic nerves as the experimental model, ultrasound-guided injections of free ropivacaine, PRMs, and APRMs with equivalent concentrations were performed (Figure 4c). Precise localization of the target sciatic nerve was achieved through ultrasonographic imaging (Figure 4d(i)), ensuring accurate therapeutic delivery. Following this, the drugs were administered under continuous ultrasound visualization. As demonstrated in Figure 4d(ii), ultrasonographic imaging of free ropivacaine revealed an anechoic region, characterized by the absence of echo signals. In contrast, the ultrasonographic imaging of PRMs and APRMs in Figure 4d(iii) and Figure 4d(iv) exhibited strong echogenic spots, attributable to the hollow bubble structures. These findings demonstrate that the APRMs possess CEUS properties, which are critical for precise and targeted drug delivery.

Tissue Adhesion

In vivo visualization of the three formulations was enabled through Cy5.5 labeling of PRMs and APRMs, with ropivacaine administered in a Cy5.5-containing solution. Fluorescence imaging was conducted post-injection (0, 0.5, 1, 2, 4, 6, and 8 hours) (Figure 5a). The fluorescence signal from Cy5.5-labeled ropivacaine demonstrated time-dependent spatial expansion, while Cy5.5-labeled APRMs exhibited consistent fluorescence distribution patterns throughout the observation (Supplementary Table 2). The fluorescence distribution of PRMs remained unchanged until 6 hours, displayed rapid expansion at the 6-hour mark, and subsequently diminished by 8 hours post-injection (Figure 5b). After the 8-hour experimental period, rats were euthanized, and major organs were extracted for subsequent evaluation. Ex vivo imaging of collected organs (Figure 5c) demonstrated higher fluorescence intensity following ropivacaine treatment than PRMs and APRMs treatment groups in liver and kidney tissues (Figure 5d).

Tissue adhesion properties were further investigated using Sudan blue II-labeled PRMs and APRMs, with ropivacaine delivered as a black water-soluble dye solution. Sciatic nerve blockade was conducted in rat models, with subsequent evaluation of perineural drug diffusion patterns through sciatic nerve exposure on post-injection day 5. The results indicated significantly more extensive diffusion areas for ropivacaine and PRMs compared to APRMs (Figure 5e), indicating that APRMs exhibited stronger tissue adhesion than PRMs and ropivacaine. Overall, the enhanced adhesion of APRMs ensured more stable drug retention at the target site, improved drug bioavailability, and reduced systemic toxicity.

Effect of Perisciatic Nerve Injection

To evaluate the sustained analgesic efficacy of APRMs, we assessed the ipsilateral sciatic nerves in adult male rats after implementation of surgical incision and SNI-induced neuropathic pain models. A plantar incision was created, followed by sciatic nerve block. The plantar incision model, originally designed for acute postoperative pain research, could closely mimic human postoperative pain experience.[27] Mechanical and thermal nociceptive hypersensitivities were evaluated on the ipsilateral side in each group (Figure 6a and b). PRMs and APRMs exhibited significantly extended analgesic efficacy during the maintenance period, up to 4 days post-administration (Figure 6c). In contrast to the sustained effects of PRMs and APRMs, free ropivacaine exhibited transient analgesia lasting only 24 hours post-incision, consistent with its clinical efficacy profile. As expected, administration of vehicle control or PLGA alone failed to demonstrate significant effects on mechanical allodynia or thermal hyperalgesia. However, the precise duration of efficacy has yet to be fully established in this acute pain model. To address this issue, we designed a chronic pain model induced by SNI to evaluate their long-term analgesic potential. Consequently, APRMs exhibited a pronounced and sustained antinociceptive activity, maintaining 15 days for thermal analgesia and 9 days for mechanical analgesia (Figure 6d). Although PRMs demonstrated a 3-day shorter duration of thermal analgesia compared to APRMs (adjusted $P=0.938$ on day 25 after SNI surgery), their mechanical analgesic efficacy was comparable to that of APRMs (adjusted $P>0.99$ on day 25 after SNI surgery) (Figure 6d). Free ropivacaine demonstrated limited analgesic duration, with mechanical effects lasting 24 hours and thermal effects persisting for only 4 hours. Consistent with the plantar incision model, vehicle control and PLGA alone injections showed no significant effects on analgesia (Supplementary Table 3).

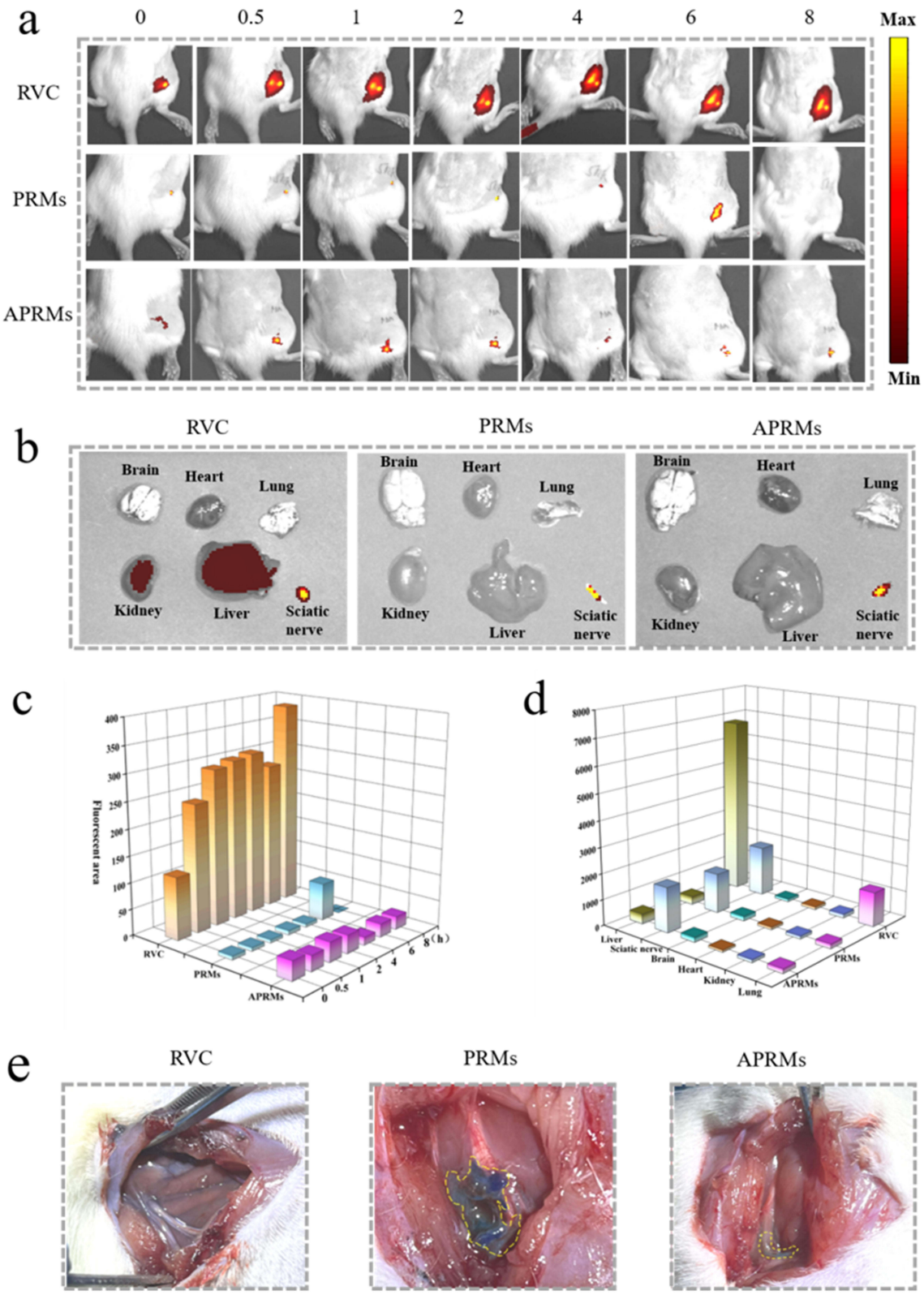

Figure 5 (**a**) Representative in vivo images and (**b**) quantified fluorescence signals of different drug formulations at various time points post-injection. (**c**) Representative ex vivo images of tissues following treatment. Groups: i: ropivacaine, ii: PRMs, iii: APRMs. (**d**) Quantitative analysis of fluorescence intensity in major organs following 8-hour post-administration of ropivacaine, PRMs, and APRMs in rat models. RVC: ropivacaine. (**e**) Tissue visualization of sciatic nerve after injections, with yellow circular annotations indicating drug dispersion areas.

https://doi.org/10.2147/DDDT.S532749

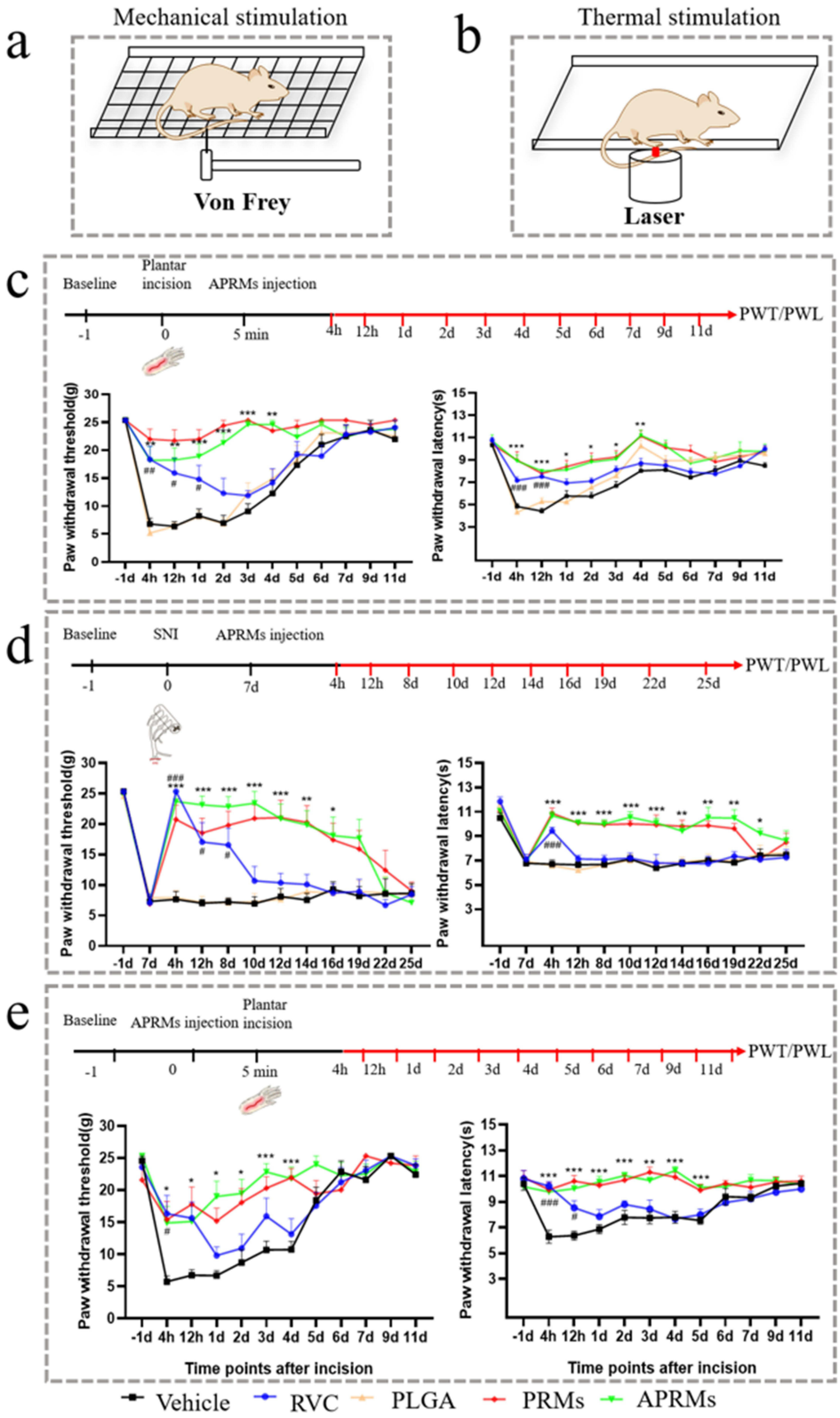

Figure 6 (**a**) Schematic diagram of mechanical stimulation. (**b**) Schematic diagram of thermal stimulation. (**c**) Mechanical and thermal nociceptive responses in a rat plantar incision model at various time points. (**d**) Mechanical and thermal nociceptive responses in an SNI model. (**e**) Preventive analgesic effects of vehicle, ropivacaine, PRMs, and APRMs on mechanical and thermal nociception prior to plantar incision. Data presented as mean ± SEM (n = 8 rats/group). **P*<0.05, ***P*<0.01, ****P*<0.001 APRMs vs vehicle; $^{\#}P$<0.05, $^{\#\#}P$<0.01, $^{\#\#\#}P$<0.001 RVC vs vehicle.

https://doi.org/10.2147/DDDT.S532749

These results indicate that APRMs exhibited extended analgesic duration, potentially attributable to the enhanced tissue adhesion conferred by the polydopamine coating.

The preventive analgesic properties of APRMs were assessed in a plantar incision model, with pre-emptive sciatic nerve blockade achieved. The analgesic efficacy was quantitatively assessed during the development period, as illustrated in Figure 6e. APRMs demonstrated significant enhancement of PWT and PWL, with effects persisting through postoperative day 5. Free ropivacaine showed limited analgesic duration (12 hours), whereas vehicle injection had no significant impact on nociceptive responses.

These findings underscore the remarkable and extended analgesic efficacy of APRMs, suggesting their viability as a promising treatment strategy in pain management.

Safety Evaluations

Comprehensive safety evaluation of APRMs was conducted. Locomotor function assessment demonstrated transient reductions in placing and grasping reflex scores at the 2-hour post-injection time point across different treatment groups (Supplementary Table 4). While placing and grasping reflex scores showed temporary reductions, they returned to normal at later time points, and righting reflex remained stable across all time points in all groups (Supplementary Table 4). To assess histopathology, Hematoxylin and Eosin (H&E) staining and histological examination were performed after injection of ropivacaine, PRMs and APRMs. Post-treatment analysis showed normal wound healing with no signs of delayed healing or muscle atrophy (Figure S3). At 11 days post-injection, the exposed sciatic nerves remained intact, exhibiting normal morphology across all groups, including ropivacaine, PRMs, and APRMs (Figure S4). Histological assessment using HE staining demonstrated maintained sciatic nerve adventitial integrity, with normal myelinated fiber morphology and distribution. The sciatic nerve fibers were tightly arranged, uniformly distributed, and densely myelinated, with fully developed axons. No signs of axonal swelling or atrophy were observed in any group. All groups showed normal axonal morphology without evidence of swelling or atrophy (Figure 7a). Transmission electron microscope (TEM) further confirmed these findings, revealing abundant and intact myelinated fibers with normal axonal structure in all groups (Figure 7b). Some sections showed minor myelin sheath layer separation, but no significant differences were detected among the four groups (Figure 7b). Furthermore, visceral toxicity was assessed via HE staining of major organs on day 11 post-perisciatic injection. The results (Figure 8) revealed no pathological changes among the groups, further confirming the safety of APRMs.

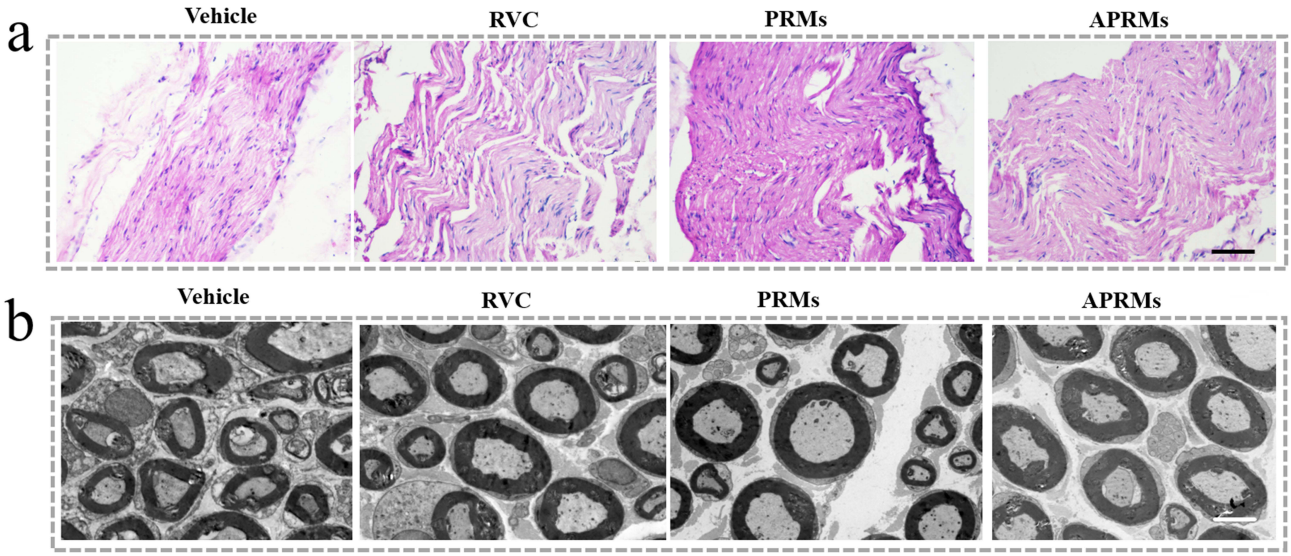

Figure 7 (**a**) HE stained sections of sciatic nerve 11 days post-perisciatic administration of vehicle, ropivacaine, PRMs, and APRMs. The scale bar is 100 μm. (**b**) TEM images of sciatic nerve tissue 11 days post-perisciatic injection of vehicle, ropivacaine, PRMs, or APRMs. The scale bar is 10 μm.

https://doi.org/10.2147/DDDT.S532749

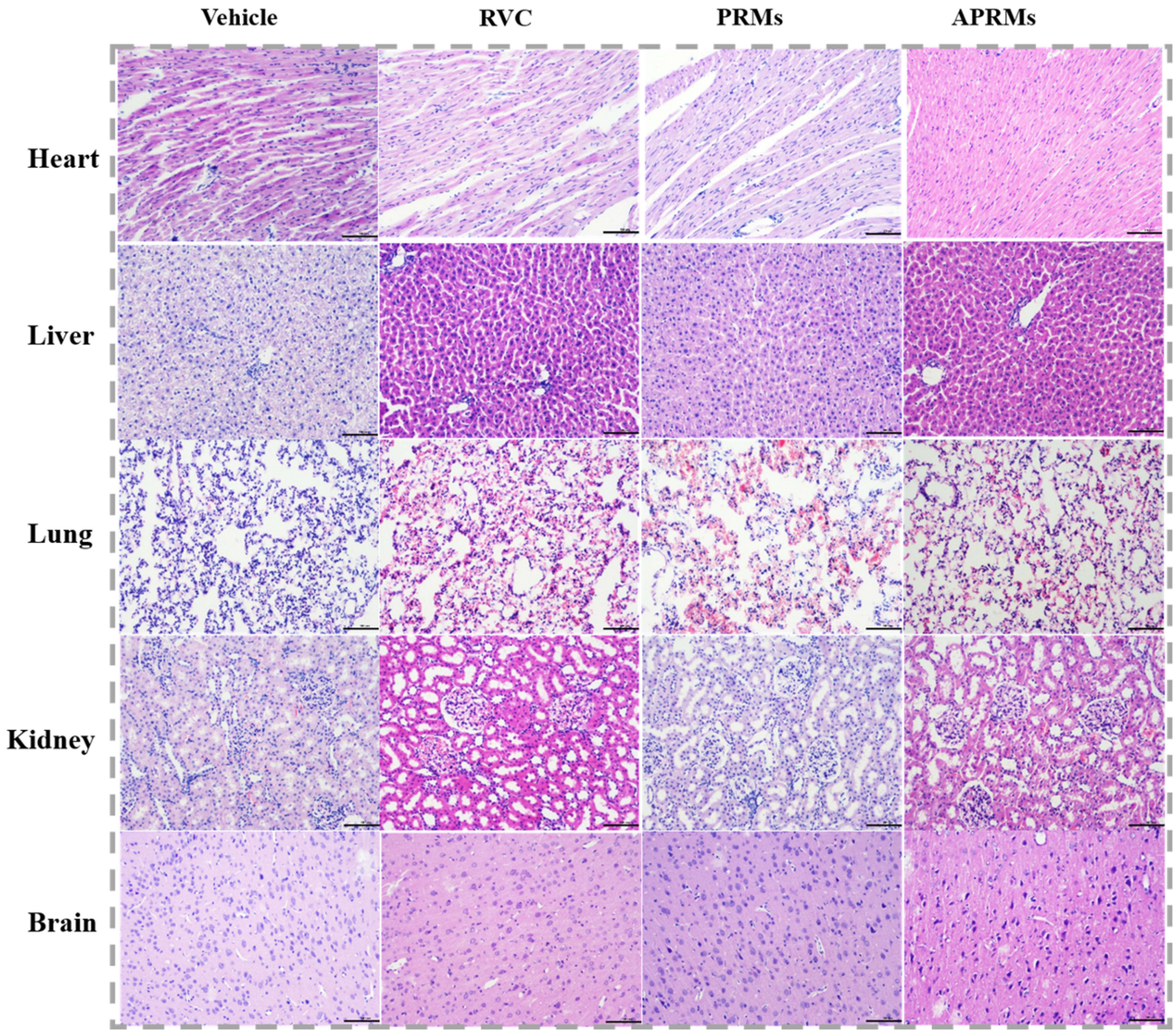

Figure 8 HE-stained tissue sections of heart, liver, lung, kidney and brain 11 days post-perisciatic nerve injections. Scale bar: 100 μm.

Discussion

To our knowledge, this is the first to put forward the concept of mussel protein inspired adhesive CEUS ropivacaine formulation for regional anesthesia. Ropivacaine loaded adhesive PLGA microbubbles were successfully fabricated in this study. The analgesic efficacy of APRMs is primarily attributed to several interrelated mechanisms. First, the polydopamine coating endows the microbubbles with mussel protein-inspired adhesive properties, enhancing local retention at the injection site and reducing rapid drug diffusion. Second, the PLGA microbubble structure allows sustained release of ropivacaine, providing prolonged sensory blockade while minimizing motor impairment. Third, the contrast-enhanced ultrasonography capability enables real-time visualization of the microbubbles, facilitating precise targeting and monitoring of drug delivery. Collectively, this study introduces a new and effective drug option for pain management, offering promising applications.

Polydopamine, recognized for its superior biocompatibility, inherent adhesive characteristics, photothermal capabilities, and anti-inflammatory properties, finds extensive applications in biomedical domains. It serves various functions, including drug delivery,[32,33] tissue repair,[34,35] and therapeutic applications.[36,37] In this study, polydopamine was employed as a coating material for APRMs, enhancing their mussel protein inspired adhesive properties and improving

https://doi.org/10.2147/DDDT.S532749

drug targeting at specific sites. The adhesive properties of APRMs enable more stable drug targeting, lowering dosage and toxicity risks. Tissue-adhesive local anesthetics effectively bind to surfaces like oral mucosa or skin, ideal for topical anesthesia. However, the behavioural differences observed between the APRMs and PRMs groups were not statistically significant, possibly due to variations in encapsulation and drug-loading efficiencies. In addition, heterogeneity in the intervention, such as microbubble size distribution and local retention at the injection site, may have contributed to inter-subject variability. Furthermore, inter-individual differences, including metabolic rates, tissue composition, and immune responses, could influence drug release kinetics and analgesic efficacy. These findings underscore the importance of considering both formulation characteristics and patient-specific factors when evaluating therapeutic outcomes. Importantly, this variability highlights the potential for developing targeted or precision medicine strategies, where individualized dosing regimens and optimized delivery systems could maximize efficacy while minimizing variability in treatment response. Notably, APRMs exhibited a relatively short motor block duration, suggesting their ability to provide long-term sensory blockade while minimizing motor impairment.

To achieve simultaneous drug loading and ultrasound contrast capabilities, this study utilized a hollow spherical structure. While microbubbles have been previously reported for CEUS applications,[38] these were generally smaller in size and designed for focal contrast.[39,40] In contrast, the larger microbubbles in this study were primarily developed for drug delivery and sustained release in regional anesthesia. The ultrasound contrast of APRMs is based on the acoustic impedance difference between the hollow structure and the surrounding medium.[40] Therefore, porous or mesoporous structures leveraging acoustic impedance differences may achieve similar ultrasound contrast effects as APRMs. Future studies could explore this approach. In this study, no adverse events were observed, indicating a favorable safety profile under the experimental conditions. Nevertheless, ongoing monitoring of safety parameters, including both clinical signs and relevant biomarkers, is warranted in future preclinical and clinical studies. Systematic assessment of these endpoints will provide a more comprehensive understanding of risk profiles and support the safe translation of APRMs into clinical applications. Moreover, incorporating safety considerations into the design of delivery systems and dosing regimens may further enhance therapeutic efficacy while minimizing potential adverse effects.

We acknowledge several limitations in the present study. First, only male Sprague-Dawley rats were used, which may limit the generalizability of our findings. Future studies should include female subjects and other species to better evaluate potential sex- and species-related differences in drug distribution, analgesic efficacy, and safety. Second, histopathological and neurotoxicity evaluations were conducted only on the day 11, which does not exclude the possibility of longer-term inflammation or fibrosis. We have clarified this limitation and emphasize that extended time points will be included in future studies to comprehensively evaluate chronic tissue responses and safety. Third, the relatively low encapsulation efficiency (EE = 23.1%) of APRMs may require higher doses to achieve therapeutic effects, and the safety of higher-load microbubbles remains to be fully evaluated. In the current study, doses were within the safe range determined in preliminary toxicity assessments, with no adverse effects observed. Future work will focus on optimizing encapsulation efficiency and evaluating the toxicity profile of higher-load APRMs to maximize efficacy while minimizing potential risks. Addressing these limitations will further enhance the translational relevance of APRMs for clinical pain management.

Conclusion

In summary, this study developed a mussel protein inspired adhesive microbubble drug delivery system that combines CEUS imaging capabilities with sustained analgesic effects in preclinical models of regional anesthesia. These findings demonstrate the potential of this microbubble delivery strategy to provide controlled and localized analgesia. While promising, further investigations, including first-in-human studies and Phase 1 clinical trials, are necessary to evaluate safety, tolerability, and efficacy before clinical translation can be considered.

Acknowledgments

We would like to thank the professors of the School of Basic Medical Sciences, Zhengzhou University, for their valuable assistance and support in this project.

Funding

This work was supported by the National Natural Science Foundation (No.82101279), Zhongyuan Science, and Technology Innovation Leadership Program of Henan Province, China (Grant No. ZYYCYU202012030), and Henan Medical Science and Technology Project (No. LHGJ20200295).

Disclosure

The authors report no conflicts of interest in this project.

References

1. White PF. Cost-effective multimodal analgesia in the perioperative period: use of intravenous vs. oral Acetaminophen. *J Clin Anesth*. 2020;61:109625. doi:10.1016/j.jclinane.2019.109625
2. Plein LM, Rittner HL. Opioids and the immune system – friend or foe. *Br J Pharmacol*. 2018;175(14):2717–2725. doi:10.1111/bph.13750
3. Rawal N. Current issues in postoperative pain management. *Eur J Anaesthesiol*. 2016;33(3):160–171. doi:10.1097/EJA.0000000000000366
4. Warman P, Nicholls B. Ultrasound-guided nerve blocks: efficacy and safety. *Best Pract Res Clin Anaesth*. 2009;23(3):313–326. doi:10.1016/j.bpa.2009.02.004
5. Peterson MK, Millar FA, Sheppard DG. Editorial I. *Br J Anaesth*. 2002;88(5):621–624. doi:10.1093/bja/88.5.621
6. Joshi G, Gandhi K, Shah N, Gadsden J, Corman SL. Peripheral nerve blocks in the management of postoperative pain: challenges and opportunities. *J Clin Anesth*. 2016;35:524–529. doi:10.1016/j.jclinane.2016.08.041
7. Jeng CL, Torrillo TM, Rosenblatt MA. Complications of peripheral nerve blocks. *Br J Anaesth*. 2010;105:i97–i107. doi:10.1093/bja/aeq273
8. Li L, Zhao Y, Guo L, Lv X, Yu G. Ultrasound guidance enhances the efficiency of brachial plexus block and ameliorates the vascular injury compared with nerve stimulator guidance in hand surgery patients. *J Invest Surg*. 2020;33(6):530–535. doi:10.1080/08941939.2018.1539792
9. Liu Y, Mei W. Enhanced needle visibility by micro air bubble contrast in ultrasound-guided nerve block. *Anesthesiology*. 2018;128(6):1238. doi:10.1097/ALN.0000000000002084
10. Lirk P, Hollmann MW, Strichartz G. The science of local anesthesia. *Anesthesia Analg*. 2018;126(4):1381–1392. doi:10.1213/ANE.0000000000002665
11. Desai N, Kirkham KR, Albrecht E. Local anaesthetic adjuncts for peripheral regional anaesthesia: a narrative review. *Anaesthesia*. 2021;76(S1):100–109. doi:10.1111/anae.15245
12. Ilfeld BM. Continuous peripheral nerve blocks. *Anesthesia Analg*. 2017;124:308–335. doi:10.1213/ANE.0000000000001581
13. Krishna Prasad G, Khanna S, Jaishree S. Review of adjuvants to local anesthetics in peripheral nerve blocks: current and future trends. *Saudi J Anaesth*. 2020;14(1):77–84. doi:10.4103/sja.SJA_423_19
14. Liu GL, Bian WC, Zhao P, Sun LH. Delivery of local anesthesia: current strategies, safety, and future prospects. *Curr Drug Metab*. 2019;20(6):533–539. doi:10.2174/1389200220666190610155049
15. Santamaria CM, Woodruff A, Yang R, Kohane DS. Drug delivery systems for prolonged duration local anesthesia. *Mater Today*. 2017;20(1):22–31. doi:10.1016/j.mattod.2016.11.019
16. Danhier F, Ansorena E, Silva JM, Coco R, Le Breton A, Préat V. PLGA-based nanoparticles: an overview of biomedical applications. *J Control Release*. 2012;161(2):505–522. doi:10.1016/j.jconrel.2012.01.043
17. Swider E, Koshkina O, Tel J, Cruz LJ, de Vries IJM, Srinivas M. Customizing poly (lactic-co-glycolic acid) particles for biomedical applications. *Acta Biomater*. 2018;73:38–51. doi:10.1016/j.actbio.2018.04.006
18. Kapoor DN, Bhatia A, Kaur R, Sharma R, Kaur G, Dhawan S. PLGA: a unique polymer for drug delivery. *Ther Deliv*. 2015;6(1):41–58. doi:10.4155/tde.14.91
19. Biondi M, Ungaro F, Quaglia F, Netti PA. Controlled drug delivery in tissue engineering. *Adv Drug Deliv Rev*. 2008;60(2):229–242. doi:10.1016/j.addr.2007.08.038
20. Tian X, Zhu H, Du S, et al. Injectable PLGA-coated ropivacaine produces a long-lasting analgesic effect on incisional pain and neuropathic pain. *J Pain*. 2021;22(2):180–195. doi:10.1016/j.jpain.2020.03.009
21. Ohri R, Wang JC-F, Blaskovich PD, et al. Inhibition by Local Bupivacaine-Releasing Microspheres of Acute Postoperative Pain from Hairy Skin Incision. *Anesthesia Analg*. 2013;117(3):717–730. doi:10.1213/ANE.0b013e3182a00851
22. Ohri R, Blaskovich P, Wang JC-F, et al. Prolonged nerve block by microencapsulated bupivacaine prevents acute postoperative pain in rats. *Reg Anesth Pain Med*. 2012;37(6):607–615. doi:10.1097/AAP.0b013e3182680f35
23. Tan X, Ke P, Chen Z, et al. Construction of injectable micron-sized polymorphic vesicles for prolonged local anesthesia with weekly sustained release of ropivacaine. *Int J Pharm*. 2024;661:124378. doi:10.1016/j.ijpharm.2024.124378
24. Simpson D, Curran MP, Oldfield V, Keating GM. Ropivacaine: a review of its use in regional anaesthesia and acute pain management. *Drugs*. 2005;65:2675–2717. doi:10.2165/00003495-200565180-00013
25. Ho C, Ding S. Structure, properties and applications of mussel-inspired polydopamine. *J Biomed Nanotechnol*. 2014;10(10):3063–3084. doi:10.1166/jbn.2014.1888
26. Wang W, Tang Z, Zhang Y, Wang Q, Liang Z, Zeng X. Mussel-inspired polydopamine: the bridge for targeting drug delivery system and synergistic cancer treatment. *Macromol Biosci*. 2020;20:2000222. doi:10.1002/mabi.202000222
27. Brennan TJ, Vandermeulen EP, Gebhart GF. Characterization of a rat model of incisional pain. *Pain*. 1996;64(3):493–502. doi:10.1016/0304-3959(95)01441-1
28. Decosterd I, Woolf CJ. Spared nerve injury: an animal model of persistent peripheral neuropathic pain. *Pain*. 2000;87(2):149–158. doi:10.1016/S0304-3959(00)00276-1
29. Chaplan SR, Bach FW, Pogrel JW, Chung JM, Yaksh TL. Quantitative assessment of tactile allodynia in the rat paw. *J Neurosci Methods*. 1994;53(1):55–63. doi:10.1016/0165-0270(94)90144-9

30. Hargreaves K, Dubner R, Brown F, Flores C, Joris J. A new and sensitive method for measuring thermal nociception in cutaneous hyperalgesia. *Pain*. 1988;32(1):77–88. doi:10.1016/0304-3959(88)90026-7
31. Coderre TJ, Van Empel I. The utility of excitatory amino acid (EAA) antagonists as analgesic agents. I. Comparison of the antinociceptive activity of various classes of EAA antagonists in mechanical, thermal and chemical nociceptive tests. *Pain*. 1994;59:345. doi:10.1016/0304-3959(94)90020-5
32. Liu Y, Choi CKK, Hong H, et al. Dopamine receptor-mediated binding and cellular uptake of polydopamine-coated nanoparticles. *ACS Nano*. 2021;15(8):13871–13890. doi:10.1021/acsnano.1c06081
33. Wang Z, Duan Y, Duan Y. Application of polydopamine in tumor targeted drug delivery system and its drug release behavior. *J Control Release*. 2018;290:56–74. doi:10.1016/j.jconrel.2018.10.009
34. Zhou L, Xi Y, Xue Y, et al. Injectable self-healing antibacterial bioactive polypeptide-based hybrid nanosystems for efficiently treating multidrug resistant infection, skin-tumor therapy, and enhancing wound healing. *Adv Funct Mater*. 2019;29(22):1806883. doi:10.1002/adfm.201806883
35. Xi Y, Ge J, Wang M, et al. Bioactive anti-inflammatory, antibacterial, antioxidative silicon-based nanofibrous dressing enables cutaneous tumor photothermo-chemo therapy and infection-induced wound healing. *ACS Nano*. 2020;14(3):2904–2916. doi:10.1021/acsnano.9b07173
36. Guan Q, Guo R, Huang S, et al. Mesoporous polydopamine carrying sorafenib and SPIO nanoparticles for MRI-guided ferroptosis cancer therapy. *J Control Release*. 2020;320:392–403. doi:10.1016/j.jconrel.2020.01.048
37. Bao X, Zhao J, Sun J, Hu M, Yang X. Polydopamine nanoparticles as efficient scavengers for reactive oxygen species in periodontal disease. *ACS Nano*. 2018;12(9):8882–8892. doi:10.1021/acsnano.8b04022
38. Ajmal S. Contrast-enhanced ultrasonography: review and applications. *Cureus*. 2021;13(9):e18243. doi:10.7759/cureus.18243
39. Yang F, Wang Q, Gu Z, Fang K, Marriott G, Gu N. Silver nanoparticle-embedded microbubble as a dual-mode ultrasound and optical imaging probe. *ACS Appl Mater Interfaces*. 2013;5(18):9217–9223. doi:10.1021/am4029747
40. Wang G, Song L, Hou X, et al. Surface-modified GVs as nanosized contrast agents for molecular ultrasound imaging of tumor. *Biomaterials*. 2020;236:119803. doi:10.1016/j.biomaterials.2020.119803